Supplementary Information (SI) for Chemical Science.

Partial thermal atomization of residual Ni NPs in single-walled carbon nanotubes for efficient CO_2 electroreduction

Fengwei Zhang [a‡*], Han Zhang [a‡], Yang Zhao [b], Jingjing Li [c], Chong Guan [a], Jijie Li [a], Xuran Wang [a], Yuewen Mu [a], Wen-Yan Zan [a*], and Sheng Zhu [a,d*]

[a] Institute of Crystalline Materials, Institute of Molecular Science, Key Lab of Materials for Energy Conversion and Storage of Shanxi Province, Key Laboratory of Chemical Biology and Molecular Engineering of Education Ministry, Shanxi University, Taiyuan 030006, P. R. China

[b] Dalian National Laboratory for Clean Energy, Dalian Institute of Chemical Physics, Chinese Academy of Sciences, Dalian 116023, Liaoning, P. R. China

[c] Research Institute of Resource-based Economy Transformation and Development, Shanxi University of Finance and Economics, Taiyuan 030006, P. R. China

[d] Institute for Carbon-Based Thin Film Electronics, Peking University, Shanxi (ICTFE-PKU), Taiyuan 030012, China

***Corresponding Authors.** E-mail: fwzhang@sxu.edu.cn; zanwy@sxu.edu.cn; shengzhu@sxu.edu.cn

[1] These authors contributed equally to this work

Materials and reagents

Single-walled carbon nanotubes (SWNTs, length 1~5 μm) were purchased from Nanjing XFNANO Materials Tech Co., Ltd., formamide and potassium bicarbonate ($KHCO_3$) were provided by Macklin Biochemical Co., Ltd. Anhydrous ethanol (EtOH) and *N*, *N*-dimethylformamide (DMF) were obtained from Meryer Co., Ltd. All of other reagents were used directly and without any treatment.

CO_2 electroreduction measurements

Electrochemical tests were conducted using a CHI 660E electrochemical workstation from CH Instruments, under ambient temperature and pressure in a three-electrode system. A platinum sheet served as the anode, a saturated Ag/AgCl electrode was used as the reference electrode, and a glassy carbon working electrode coated with the catalyst served as the cathode. An H-type electrolytic cell containing 0.5 M $KHCO_3$ was used as the electrolyte solution. Before the electrochemical tests, CO_2 was bubbled into the $KHCO_3$ solution at a flow rate of 40 mL/min for 0.5 hours to saturate the electrolyzer with CO_2. During the tests, a continuous CO_2 flow of 20 mL/min was maintained through the catholyte, and each potential was subjected to potentiostatic electrolysis for 0.5 hours. All potentials were referenced to the reversible hydrogen electrode (RHE) using the following equation: $E_{RHE} = E°_{Ag/AgCl}\ (0.20\ V) + E_{Ag/AgCl} + 0.059 \times pH$. The gaseous products were collected using a gas bag and analyzed with an HXSP GC-950 gas chromatograph equipped with two thermal conductivity detectors (TCD) and a flame ionization detector (FID), using helium as the internal standard. Under constant temperature and pressure, 20 mL of the gas product from a gas bag (approximately 2.0 L) was injected into the GC using a sampling syringe. The mole fractions of CO and H_2 were determined from the GC calibration curve. After 1 hour of potentiostatic electrolysis, liquid products were quantified using proton nuclear magnetic resonance (1H NMR, Bruker 400 MHz) with water peak suppression. The reported results are the averages of three trials.

Electrochemical impedance spectroscopy (EIS) measurements were performed by applying an AC voltage with an amplitude of 5 mV over a frequency range from 100 kHz to 100 mHz. The stability of the functionalized single-walled carbon nanotubes (f-

SWNTs-650) catalyst was assessed by continuous electrolysis for 48 hours, with gas phase components analyzed hourly via GC. The Faradaic efficiencies (FE) of CO and H_2 and the partial current densities were calculated using the following equations:

$$\mathrm{FE}_{\mathrm{CO}} = C_{CO} \times S \times (2FP/\mathrm{RT}) / I_{\mathrm{total}} \quad \mathrm{FE}_{\mathrm{H_2}} = C_{H_2} \times S \times (2FP/RT) / I_{\mathrm{total}}$$

$$J_{\mathrm{CO}} = C_{CO} \times S \times (2FP/RT) / A \qquad J_{\mathrm{H_2}} = C_{H_2} \times S \times (2FP/RT) / A$$

where C_{CO} and C_{H_2} are the concentrations of CO and H_2 measured by GC, S is the flow rate of CO_2 (15 mL/min), F is the Faraday constant (96485 $\mathrm{C \cdot mol^{-1}}$), P is atmospheric pressure (101.3 kPa), R is the gas constant (8.314 $\mathrm{J \cdot mol^{-1} \cdot K^{-1}}$), T is thermodynamic temperature (298.15 K), A is the geometric area of the electrode, and Itotal is the measured current.

The turnover frequency (TOF) of CO formation was calculated as:

$$\mathrm{TOF}\ (\mathrm{h}^{-1}) = [(j_{\mathrm{CO}} \times S / ZF)/(m_{\mathrm{cat.}} \times w / M_{\mathrm{Ni}})] \times 3600$$

where S is the geometric area of the working electrode (cm^2), Z represents the number of electrons transferred in the reduction process at the cathode (Z = 2 for the formation of CO and H_2), mcat. is the mass of the catalyst on the glassy carbon electrode (g), w is the loading of Ni in the catalyst, and $M_{\mathrm{Ni}} = 58.69$ g mol^{-1}.

The Tafel equation is:Tafel slope was achieved from the Tafel equation:

$$\mathrm{E} = a + b lg\, (j_{CO})$$

where E is the overpotential, a is a constant, b is the Tafel slope.

DFT calculations

The spin-polarized density functional theory calculations were conducted using the Vienna Ab-initio Simulation Package (VASP)[1,2]. The electron–ion interaction was described with the projector augmented-wave pseudopotential method, and the exchange-correlation interaction was treated within the generalized gradient approximation in the Perdew-Burke-Ernzerhof formalism[3,4]. The cutoff energy of 400 eV was used. The vacuum thicknesses were more than 10 Å to avoid the interaction between periodic images. All atomic positions were allowed to relax with K-point mesh 5 × 5 × 1 until the force on each atom is less than 0.02 eV/Å.

The free energy of a pair of proton and electron ($H^+ + e^-$) can be considered as a function of applied voltage relative to RHE as $\mu(\mathrm{H}^{+})+\mu(\mathrm{e}^{-})=\frac{1}{2}\mu(\mathrm{H}_{2})\text{-e}U$, based on the CHE model[5]. Using VASPKIT, a pre- and post-processing program for the VASP code, the free energies of adsorbates and non-adsorbed gas-phase molecules with the calculated electronic energy and frequency were obtained[6]. The solvent effect has been considered for *COOH and *CO by stabilizing 0.25 and 0.10 eV, respectively[7].

The charge density difference was calculated using the following expression:

$$\Delta\rho = \rho_{\mathrm{total}} - \rho_{\mathrm{NiN_4}} - \rho_{\mathrm{Ni\ NPs}}$$

where ρ_{total} represents the charge density of NiN_4 & Ni NPs, and $\rho_{\mathrm{NiN_4}}$ and $\rho_{\mathrm{Ni\ NPs}}$ are the charge densities of the atomically dispersed NiN_4 and metallic Ni NPs, respectively.

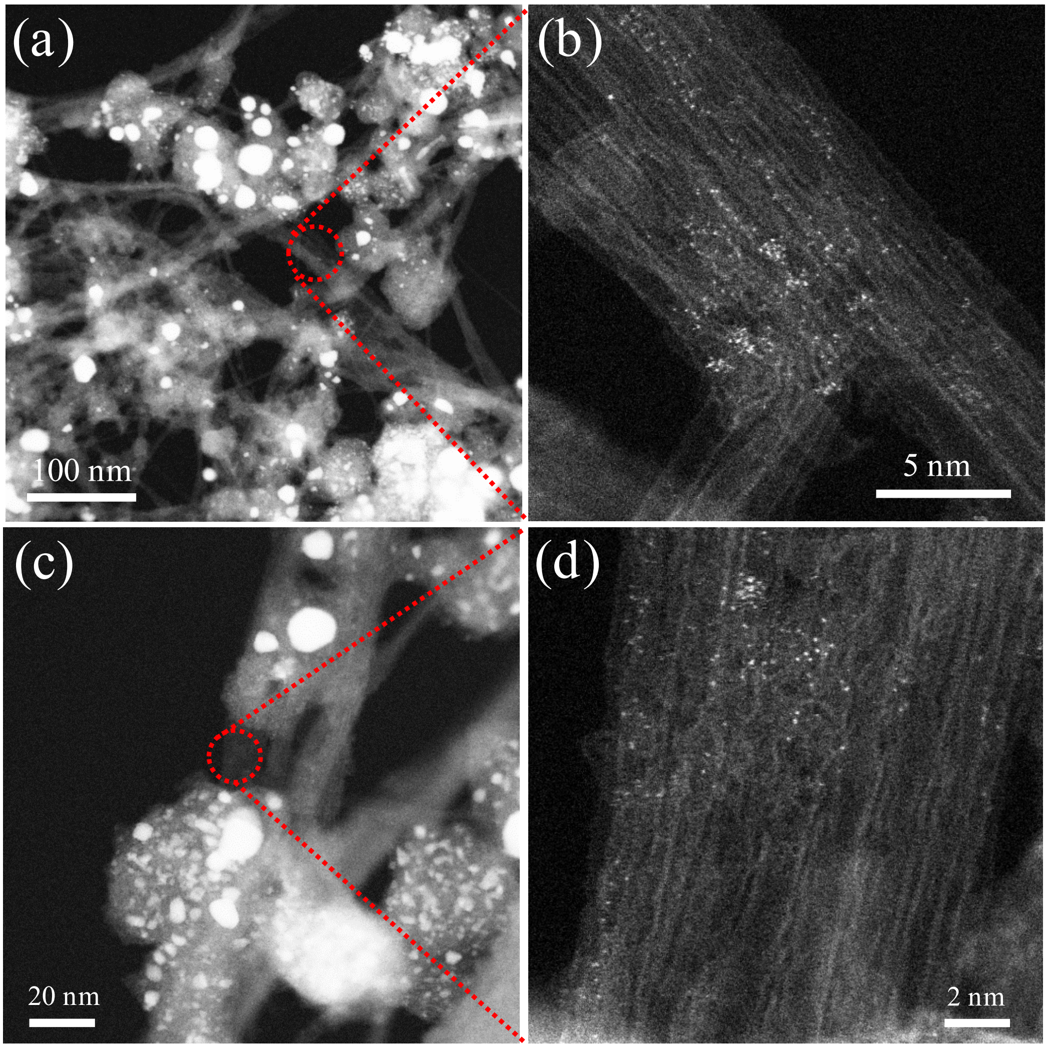

Figure S1 (a, c) HAADF-STEM images and (c, d) the corresponding high-resolution images of selected area of f-SWNTs-650 catalyst.

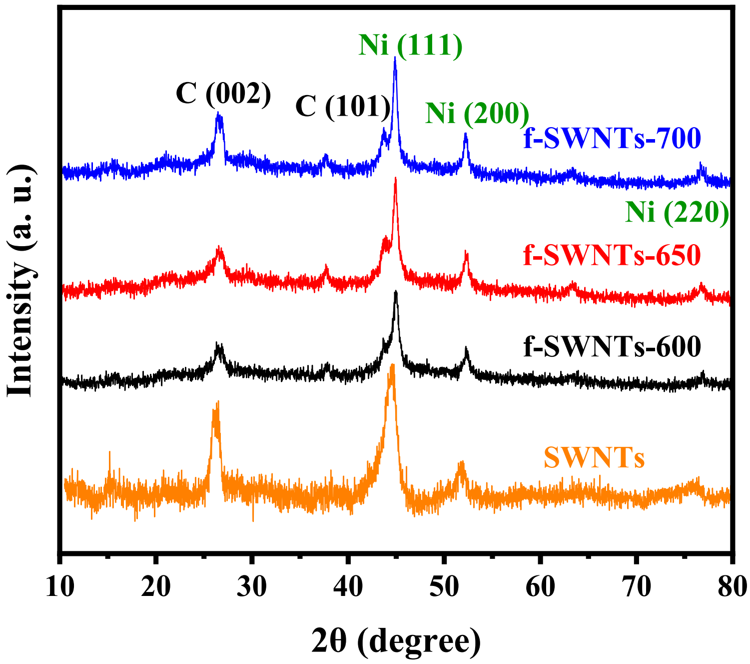

Figure S2 XRD patterns of SWNTs and f-SWNTs-T catalysts (T = 600, 650, 700 ^{o}C)

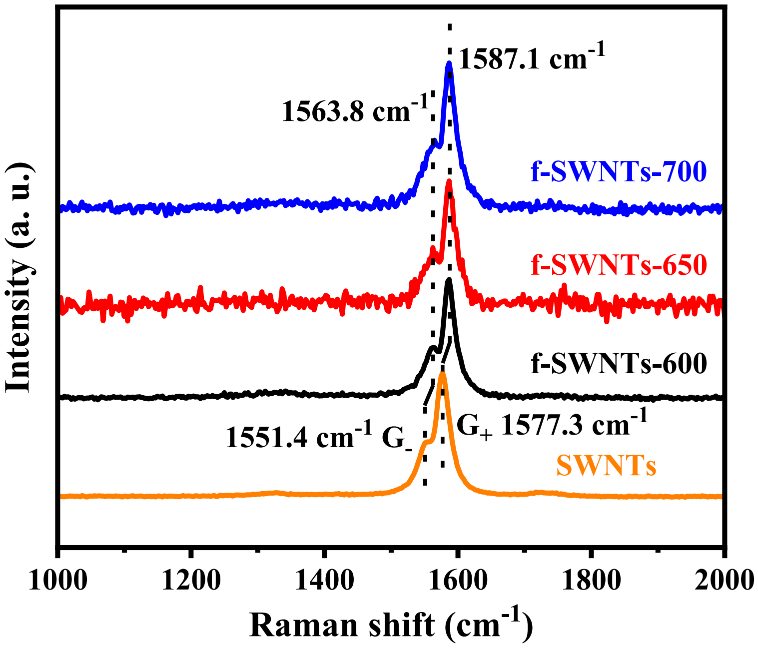

Figure S3 Raman spectra of SWNTs and f-SWNTs-T catalysts (T = 600, 650 and 700 °C)

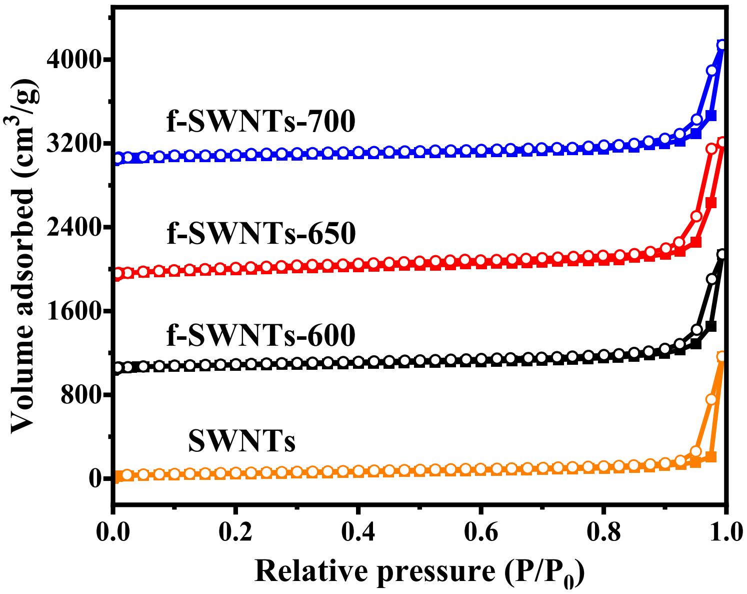

Figure S4 N_2 adsorption-desorption isotherms of SWNTs and f-SWNTs-T catalysts (T = 600, 650 and 700 °C)

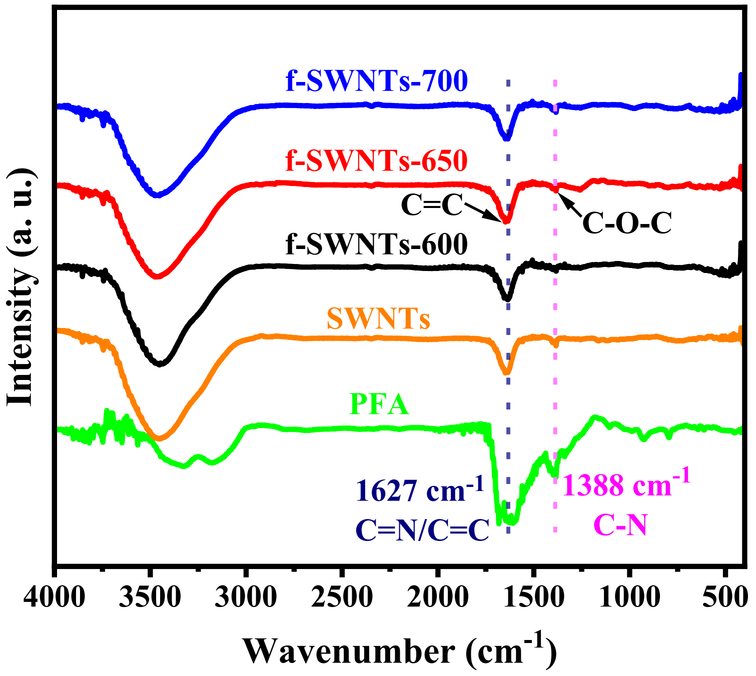

Figure S5 FTIR spectra of PFA, SWNTs and f-SWNTs-T catalysts (T = 600, 650 and 700 °C)

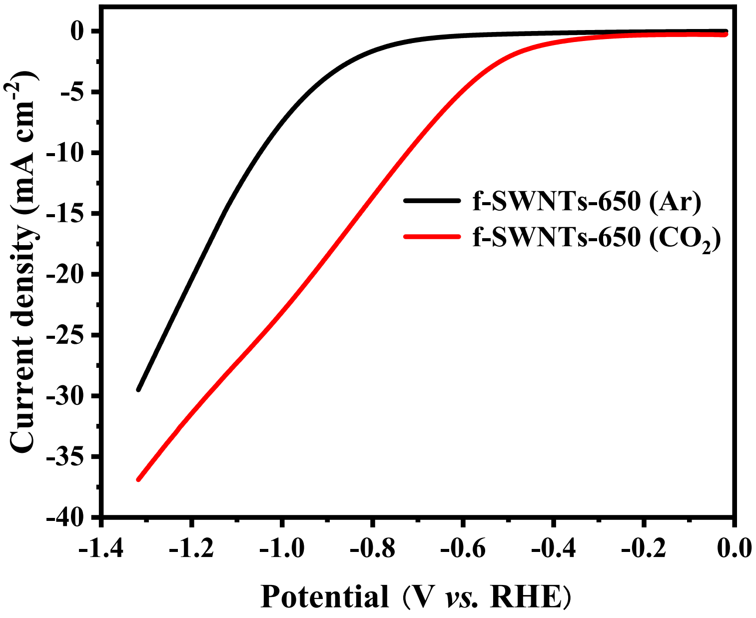

Figure S6 Linear sweep voltammetry curves of f-SWNTs-650 were collected in Ar and CO_2 saturated 0.5 M $KHCO_3$ solution.

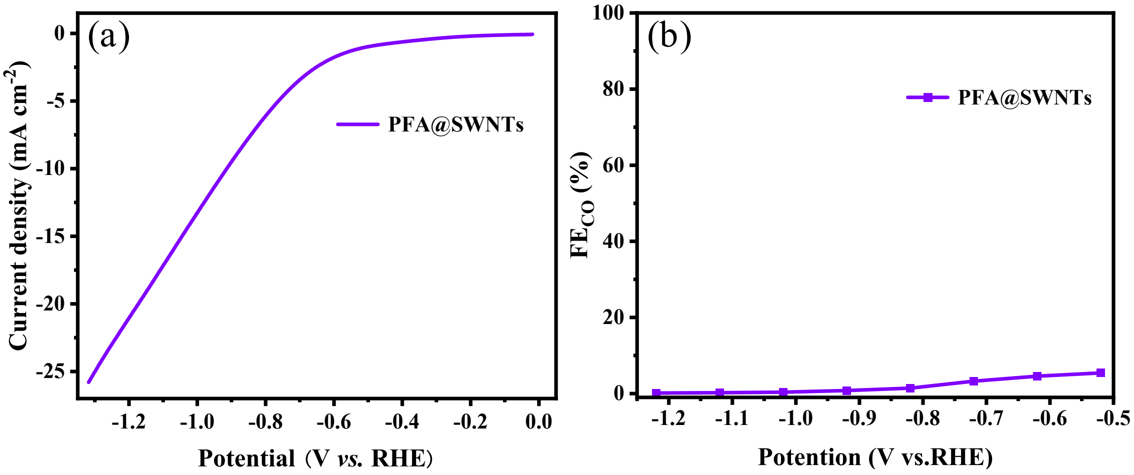

Figure S7 (a) Linear sweep voltammetry curve and FE$_{CO}$ of PFA@SWNTs sample.

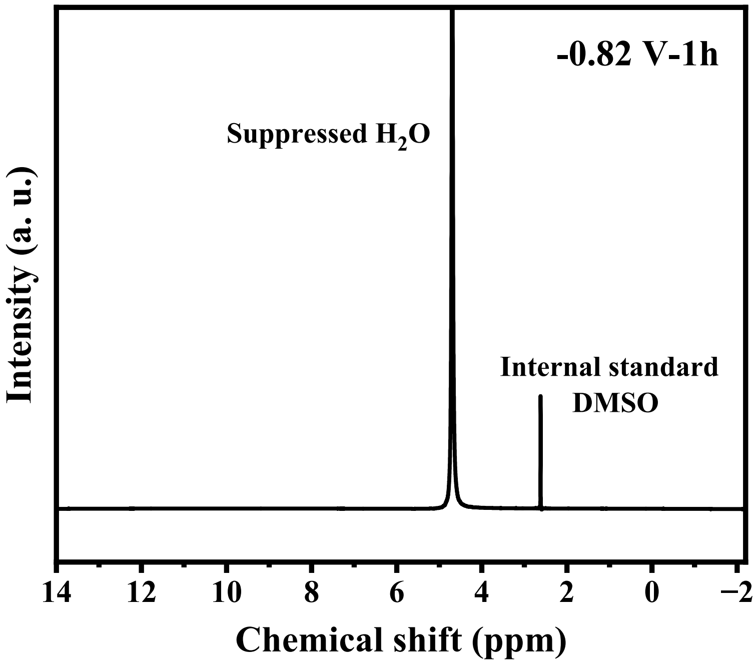

Figure S8 ^{1}H NMR spectrum of the electrolyte after 1 h CO_2 electroreduction at -0.82 V *vs*. RHE in CO_2-saturated 0.5 M $KHCO_3$ solution. There are no signal of liquid products in the electrolyte.

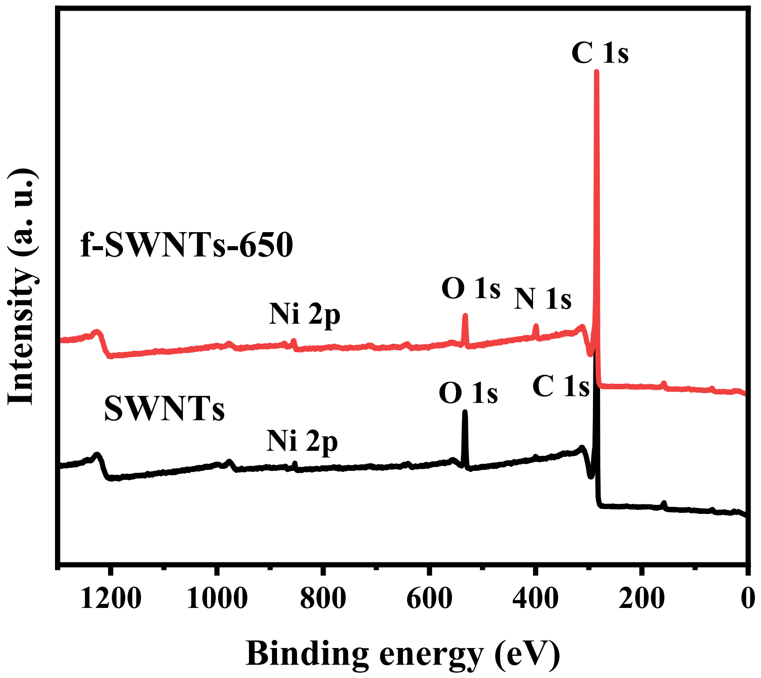

Figure S9 XPS survey scan of the pristine SWNTs and f-SWNTs-650 catalyst.

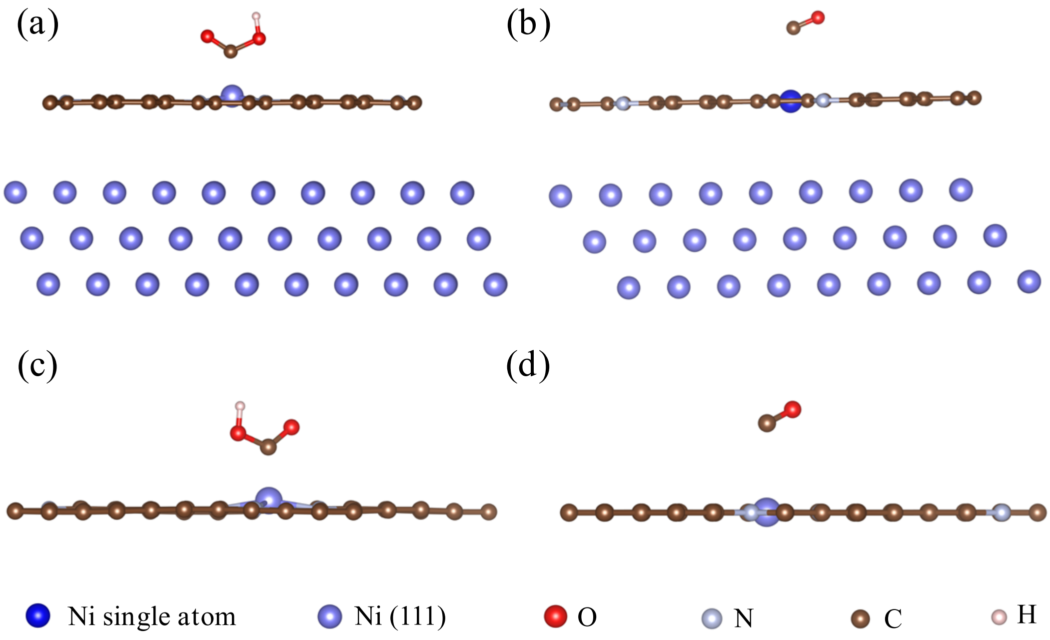

Figure S10 (a, b) Various DFT-optimized intermediates along the CO_2RR pathway over NiN_4-Ni (111) site and (c, d) Various DFT-optimized intermediates along the CO_2RR pathway over NiN_4 site.

Table S1. The results of N_2 adsorption-desorption of different samples.

Sample	Surface Area ($m^2 \cdot g^{-1}$)[a]	V ($cm^3 \cdot g^{-1}$)[b]	$\overline{D}$ (nm)[c]
SWNTs	283.1	1.332	2.98
f-SWNTs-600	295.3	1.421	2.97
f-SWNTs-650	358.9	2.086	2.13
f-SWNTs-700	297.4	1.327	2.94

[a] S_{BET} is calculated using BET method, [b] V_{total} is the single point adsorption at $P/P_0 = 0.99$,

[c] average pore diameter $\overline{D}$ is calculated using BJH method.

Table S2. EXAFS fitting parameters at the Ni K-edge for f-SWNTs-650 catalyst.

Sample	Shell	N [a]	R (Å) [b]	σ^2 (Å^2·10^{-3}) [c]	ΔE_0 (eV) [d]	*R* factor (%)
f-SWNTs-650	Ni-N	3.7	1.87	8.1	2.0	0.8
	Ni-Ni	2.5	2.48	6.0	5.4	0.8

[a] *N*: coordination numbers; [b] *R*: bond distance; [c] σ^2: Debye-Waller factors; [d] ΔE_0: the inner potential correction. *R* factor: goodness of fit. *S*02 were set as 0.85/0.89 for Ni-N/Ni-Ni , which were obtained from the experimental EXAFS fit of reference Ni foil/NiPc by fixing CN as the known crystallographic value and was fixed to all the samples.

Table S3. Summary of performance of different single atom catalyst in CO_2RR.

Catalyst	Electrolyte	Optimal Potential for selective CO generation (V *vs*.RHE)	j_{CO} (mA cm^{-2})	FEco (%)	Ref.
f-SWNTs-650	0.5 M $KHCO_3$	-0.92	-15.6	97.9	**This work**
Ni-N-C	0.5 M $KHCO_3$	-0.7	-18.5	97	[8]
NC-CNTs (Ni)	0.5 M $KHCO_3$	-1.0	-9.3	90.0	[9]
Ni-N_4-C/O	0.1 M $KHCO_3$	-0.9	-16.0	99.2	[10]
Ni-NCNT-3HS	0.5 M $KHCO_3$	-1.0	-58.0	97.4	[11]
NiAD/AgNPs@CN	0.1 M $KHCO_3$	-0.9	-4.5	99.9	[12]
NiPACN	0.1 M $KHCO_3$	-0.8	-8.0	99	[13]
Ni-N_3-C	0.5 M $KHCO_3$	-0.65	-6.6	95.6	[14]
Ni(NC)-1	0.5 M $KHCO_3$	-0.75	-10.5	99	[15]
Ni-*N*-CNTSs	0.5 M $KHCO_3$	-0.75	-5.0	95.3	[16]
Ni_1-N-C-50	0.5 M $KHCO_3$	-0.7	-7.5	94	[17]
Ni/NPC	0.1 M $KHCO_3$	-0.7	-16.0	97.2	[18]
h-Ni/N/C	0.5 M $KHCO_3$	-0.8	-21.6	96	[19]
Ni-N_4-SC	0.5 M $KHCO_3$	-0.7	-15.0	95	[20]
Ni-NC-600	0.5 M $KHCO_3$	-1.1	-12.0	99.9	[21]

References

[1] G. Kresse, J. Furthmüller, Efficient iterative schemes for *ab initio* total-energy calculations using a plane-wave basis set. Physical Review B **1996**, *54*, 11169-11186.

[2] G. Kresse, J. Furthmüller, Efficiency of ab-initio total energy calculations for metals and semiconductors using a plane-wave basis set. Computational Materials Science **1996**, *6*, 15-50.

[3] J. P. Perdew, K. Burke, M. Ernzerhof, Generalized gradient approximation made simple. Physical Review Letters **1996**, *77*, 3865-3868.

[4] J. P. Perdew, M. Ernzerhof, Rationale for mixing exact exchange with density functional approximations. Journal of Chemical Physics **1996**, *105*, 9982-9985.

[5] J. K. Nørskov, J. Rossmeisl, A. Logadottir, L. Lindqvist, J. R. Kitchin, T. Bligaard, H. Jónsson, Origin of the overpotential for oxygen reduction at a fuel-cell cathode. Journal of Physical Chemistry B **2004**, *108*, 17886.

[6] V. Wang and N. Xu, VASPKIT: A Pre- and Post-Processing Program for the VASP Code. http://vaspkit.sourceforge.net.

[7] Y. Li, H. Su, S. H. Chan, Q. Sun, CO_2 electroreduction performance of transition metal dimers supported on graphene: A theoretical study. ACS Catalysis **2015**, *5*, 6658-6664.

[8] J. Wang, Y.-C. Huang, Y. Wang, H. Deng, Y. Shi, D. Wei, M. Li, C.-L. Dong, H. Jin, S. S. Mao, S. Shen, Atomically Dispersed Metal-Nitrogen-Carbon Catalysts with d-Orbital Electronic Configuration-Dependent Selectivity for Electrochemical CO_2-to-CO Reduction. *ACS Catalysis* **2023,** *13*, 2374-2385.

[9] Q. Fan, P. Hou, C. Choi, T.-S. Wu, S. Hong, F. Li, Y.-L. Soo, P. Kang, Y. Jung, Z. Sun, Activation of Ni Particles into Single Ni–N Atoms for Efficient Electrochemical Reduction of CO_2. *Advanced Energy Materials* **2020,** *10*, 1903068.

[10] X. Wang, Y. Wang, X. Sang, W. Zheng, S. Zhang, L. Shuai, B. Yang, Z. Li, J. Chen, L. Lei, N. M. Adli, M. K. H. Leung, M. Qiu, G. Wu, Y. Hou, Dynamic Activation of Adsorbed Intermediates via Axial Traction for the Promoted Electrochemical CO_2 Reduction. *Angewandte Chemie International Edition* **2021,** *60*, 4192-4198.

[11] R. Boppella, Y. Kim, K. A. Joshi Reddy, I. Song, Y. Eom, E. Sim, T. K. Kim, Synergistic electronic structure modulation in single-atomic Ni sites dispersed on Ni nanoparticles encapsulated in N-rich carbon nanotubes synthesized at low temperature for efficient CO_2 electrolysis. *Applied Catalysis B: Environment and Energy* **2024,** *345*, 123699.

[12] Z. Zhao, L. Lin, Y. Ni, L. Jin, L. Feng, Y. Wang, Y. Wei, J. Zhang, J. Chen, Atomic level dispersed nickel coupled with silver nanoparticle to boost the efficiency of CO_2 conversion to CO via spin electrons regulation. *Applied Catalysis B: Environment and Energy* **2024,** *349*, 123886.

[13] D. M. Koshy, S. Chen, D. U. Lee, M. B. Stevens, A. M. Abdellah, S. M. Dull, G. Chen, D. Nordlund, A. Gallo, C. Hahn, D. C. Higgins, Z. Bao, T. F. Jaramillo, Understanding the Origin of Highly Selective CO_2 Electroreduction to CO on Ni,N-doped Carbon Catalysts. *Angewandte Chemie International Edition* **2020,** *59*, 4043-4050.

[14] Y. Zhang, L. Jiao, W. Yang, C. Xie, H.-L. Jiang, Rational Fabrication of Low-

Coordinate Single-Atom Ni Electrocatalysts by MOFs for Highly Selective CO_2 Reduction. *Angewandte Chemie International Edition* **2021,** *60*, 7607-7611.

[15] C. F. Wen, F. Mao, Y. Liu, X. Y. Zhang, H. Q. Fu, L. R. Zheng, P. F. Liu, H. G. Yang, Nitrogen-Stabilized Low-Valent Ni Motifs for Efficient CO_2 Electrocatalysis. *ACS Catalysis* **2020,** *10*, 1086-1093.

[16] Z. Ma, X. Zhang, D. Wu, X. Han, L. Zhang, H. Wang, F. Xu, Z. Gao, K. Jiang, Ni and nitrogen-codoped ultrathin carbon nanosheets with strong bonding sites for efficient CO_2 electrochemical reduction. *Journal of Colloid and Interface Science* **2020,** *570*, 31-40.

[17] M. Wen, N. Sun, L. Jiao, S.-Q. Zang, H.-L. Jiang, Microwave-Assisted Rapid Synthesis of MOF-Based Single-Atom Ni Catalyst for CO_2 Electroreduction at Ampere-Level Current. *Angewandte Chemie International Edition* **2024,** *63*, e202318338.

[18] R. Yun, R. Xu, C. Shi, B. Zhang, T. Li, L. He, T. Sheng, Z. Chen, Post-modification of MOF to fabricate single-atom dispersed hollow nanocages catalysts for enhancing CO_2 conversion. *Nano Research* **2023,** *16*, 8970-8976.

[19] Y. Chen, J. Zhang, J. Tian, Y. Guo, F. Xu, Y. Zhang, X. Wang, L. Yang, Q. Wu, Z. Hu, Hierarchical Ni/N/C Single-Site Catalyst Achieving Industrial-Level Current Density and Ultra-Wide Potential Plateau of High CO Faradic Efficiency for CO_2 Electroreduction. *Advanced Functional Materials* **2023,** *33*, 2214658.

[20] Q.-Q. Tang, L.-F. Feng, Z.-P. Li, S.-H. Wu, L.-S. Zhang, Q. Sun, M.-F. Wu, J.-P. Zou, Single-atom sites regulation by the second-shell doping for efficient electrochemical CO_2 reduction. *Chinese Chemical Letters* **2023**, 109454.

[21] R. Sui, B. Wang, Y. Wang, J. Pei, W. Zhu, W. Chen, C. Li, A. Sun, Z. Zhuang, A general and facile calcination method to synthesize single-site catalysts for highly efficient electrochemical CO_2 reduction. *Nano Research* **2024,** *17*, 3895-3901.